Assessing the impact of an updated spatial correlation model of ground motion parameters on the Italian Shakemap

This study was partially funded in the framework of INGV and Dipartimento della Protezione Civile (INGV-DPC) AGREEMENT B2 2019–2021, within the Task related to ShakeMap implementation in Italy. The authors thank Lucia Luzi and Alberto Michelini for their fruitful suggestions during the preparation of the work. The authors are also grateful to the two anonymous Reviewers and to the Associate Editor John Douglas for their valuable comments.

Authors:

Sara Sgobba (corresponding author), PhD - ORCID ID: 0000-0002-5669-8650

Email: sara.sgobba@ingv.it

Istituto Nazionale di Geofisica e Vulcanologia, Via Alfonso Corti, 12, 20133 Milano, Italy

Licia Faenza, PhD - ORCID ID: 0000-0002-6135-1141

Email: licia.faenza@ingv.it

Istituto Nazionale di Geofisica e Vulcanologia, Via Donato Creti, 12, 40128 Bologna, Italy

Giulio Brunelli, Dr - ORCID ID: 0000-0002-6342-7293

Email: giulio.brunelli@ingv.it

Istituto Nazionale di Geofisica e Vulcanologia, Via Alfonso Corti, 12, 20133 Milano, Italy

Giovanni Lanzano, PhD - ORCID ID: 0000-0001-7947-4281

Email: giovanni.lanzano@ingv.it

Istituto Nazionale di Geofisica e Vulcanologia, Via Alfonso Corti, 12, 20133 Milano, Italy

Abstract

This study develops a new spatial correlation model for Italy using the most up-to-date and densest dataset of accelerometer and velocimeter records available. The objective is to estimate the average correlation length and assess its impact on the prediction accuracy of the Italian Shakemap compared to the global model (Loth and Baker, 2013 - LB13) adopted in the default configuration of the program. We compute the spatial covariance structure using a geostatistical approach based on traditional variography applied to standardized residuals within the events of a reference ground motion model (ITA10). We observe spatial clusters of the correlation lengths and a wide variability over the Italian territory linked to the profound heterogeneity of the geological and geomorphological context. The obtained estimates are then implemented within the LB13 co-regionalization model in place of the default values while assuming the same cross-correlation coefficients among spectral parameters. Although our results are quite consistent with previous models calibrated for Italy, we find that the inclusion of the new correlation lengths in the Shakemap predictions, assessed through a leave-one-out cross-validation technique, results in a non-appreciable improvement over the global model, thus indicating that the adopted approach is not able to resolve the regional features and the corresponding spatial correlation with reference to individual scenarios. These findings may suggest the need to move towards nonergodic models in the Shakemap computing to better capture the spatial variability or to determine different co-regionalisation matrices more suitable for the regional applications.

Keywords: Spatial correlation; Ground motion models; Correlation length; Italian Shakemap; Shaking Intensy Measures

1. Introduction

Spatial correlation is a measure of the degree of variability of sample data in space. Its role is crucial in seismic shaking modelling, as it is known that the residuals of IMs (i.e. the difference between observations and predictions of an empirical ground motion model - GMM) - typically the within-event terms - are more correlated for closely spaced sites, due to the similarity of the seismic wave path between source and site and the homogeneity of ground conditions (Jayaram and Baker, 2009; Park et al. 2007). By definition, such spatially-varying deviations from the average predictions are not captured by the reference GMM; hence, their identification and quantification is necessary to enhance ground motion prediction capability over space and to reconstruct the shaking pattern at unobserved sites with improved accuracy. A comprehensive review of the spatial dependency of ground motion IMs and the assessment of the uncertainty in spatial-correlation models is provided by Schiappapietra and Douglas (2020) and Schiappapietra and Douglas (2021).

54 The topic is particularly relevant in many seismological applications as it has been shown to have a strong impact on the
55 estimates of probabilistic seismic hazard assessment (PSHA) and risk analysis of spatially distributed
56 structures/infrastructures (Wheatherill et al., 2015; Esposito and Iervolino, 2011; Sokolov and Wenzell, 2011; Crowley
57 et al., 2008, Park et al. 2007), as well as for emergency planning purposes and post-earthquake response, such as for the
58 Shakemap tool (Verros et al., 2017).

59 The latter is an open-source software, developed by the USGS - United States Geological Survey (Worden et al., 2018)
60 that produces near-real-time maps of shaking intensity after the occurrence of significant earthquake events. It is widely
61 used at the global level by different stakeholders including government agencies, earthquake monitoring centers, as well
62 as public and private users. Also in Italy, the ShakeMaps are produced routinely by Istituto Nazionale di Geofisica e
63 Vulcanologia (INGV) for earthquakes with magnitude≥3.0 (Michelini et al., 2008; Michelini et al., 2020) as part of the
64 products requested by the Italian Civil Protection (Dipartimento per la Protezione Civile).

65 The strategy at the base of Shakemap software combines data from individual recording stations (i.e. the recorded
66 observations in terms of IMs), empirical GMM predictions corrected for the between-event bias and site amplifications,
67 with the aim to generate a composite map of shaking (Worden et al., 2020). In doing this, the algorithm reproduces the
68 exact observation recorded at the site where the station is available. In contrast, it produces reasonable estimates at grid
69 points where data are not available by performing a geospatial interpolation of the observations via a multivariate normal
70 distribution technique (Verros et al., 2017; Worden et al. 2018). To achieve such an interpolation, it is necessary to
71 introduce a variance model that could describe the spatial dependencies in the data. In the Shakemap program, the
72 correlation function adopted is the Loth and Baker model - LB13 herein (Loth and Baker, 2013), which is one of the few
73 well-constrained models available in the literature at the global scale. This function provides both cross-correlations
74 among IMs at various periods and the spatial correlation for the same IM.

75 Although the LB13 model was calibrated on a large number of strong-motion records related to 8 large global events, its
76 estimates could be biased when applied to different tectonic and geologic contexts. It was found indeed, that the
77 correlation level is strongly influenced by regional geology and site conditions (Schiappapietra and Douglas, 2020;
78 Jayaram and Baker, 2009; Sokolov et al., 2010, Chen and Baker, 2019). Schiappapietra and Douglas also highlighted that
79 the correlation models proposed over the past two decades are affected by significant discrepancies, depending also on
80 the estimation approach of the correlation parameters (e.g. the fitting technique) and the reference GMM adopted, which
81 may lead to underestimation or overestimation of the final spatial predictions.

In this study, we want to calibrate an *ad-hoc* spatial correlation model that takes into account the peculiarities of the Italian context and evaluate the differences with LB13 implemented in the default configuration of the Shakemap programme, in order to finally assess the prediction performance on the Italian ground motion. In doing so, we focus only on the spatial correlation part of the IMs, leaving the same cross-correlations between IMs calibrated by LB13.

To this aim, we perform a geostatistical analysis of the within-event correlation structure computed with reference to a regional GMM calibrated at the national scale (ITA10, Bindi et al. 2011) in order to calibrate a new spatial model for Italy. Namely, we use traditional variography to characterize the spatial variance in the residuals and compute the *range* values (the parameter that reflects the cutoff distance between spatial dependence and spatial uncorrelation) by fitting the sample semivariogram estimators. Compared to previous models calibrated for Italy (Esposito and Iervolino, 2012; Huang and Galasso, 2019), we take advantage of the steady increase in the number of good-quality seismic records gained in the last 15 years after the occurrence of significant seismic sequences in Central and Northern Italy. A new extended Italian dataset is then used for the purpose of this work (Brunelli et al., 2022a), which benefits from the integration of a large number of velocimetric records and homogenization of the magnitude estimates that allows improved quantification of the inter-event variability, which is removed from the computation of within-event variables.

2. Dataset

The dataset adopted for the analysis is the most extended dataset available for Italy. It is extracted from the ITACA accelerometric database (ITalian ACcelerometric Archive, http://itaca.mi.ingv.it/ItacaNet_31/#/home) - version 3.1, which includes earthquakes of magnitude equal to or greater than 3.0 for the period 1972-2020 (more than 30,000 accelerometric records) only from sensors installed at ground level and in free-field conditions. In addition, this dataset includes velocimetry records with magnitudes less than 4.0 in the less sampled areas (e.g., Northwest Italy and Western Sicily), taking care to exclude recordings affected by instrument saturation. Both accelerometric and velocimetry data are manually processed according to the standard ITACA scheme, described in Paolucci et al. (2011).

Smaller events (M<4) were included in the dataset in order to extend the spatial coverage over the entire national territory, thus allowing a more homogeneous and robust sampling of the data for spatial correlation modelling. The inclusion of small events is also relevant for the application of Shakemap, since the maps in Italy are developed for events of magnitude greater than or equal to 3.0 (Michelini et al., 2020).

On this set, a selection is applied to include only events of the active crustal tectonic regime, which led to the exclusion of subduction events in the Southern Tyrrhenian Sea and volcanic events. The maximum epicentral distance for the records is 220 km, slightly higher than the validity upper threshold distance of the most common GMMs (200 km).

Several accelerometers and velocimeters are co-located, and when both recordings are available, the (not-saturated) velocimeter data is preferred with respect to the accelerometer because of the better resolution of the weak motion. This initial dataset consists of more than 37,000 records and 1,800 events.

After an additional data quality check, that resulted in the exclusion of poorly sampled events (i.e. poor azimuthal coverage or number of records ≤ 25) and poor quality records (i.e. records containing spikes or having low signal to noise ratio), we get a final dataset consisting of 25,775 records, 416 earthquakes, recorded by 1,657 measuring stations. Fig. 1 shows the events and the stations map of the final dataset.

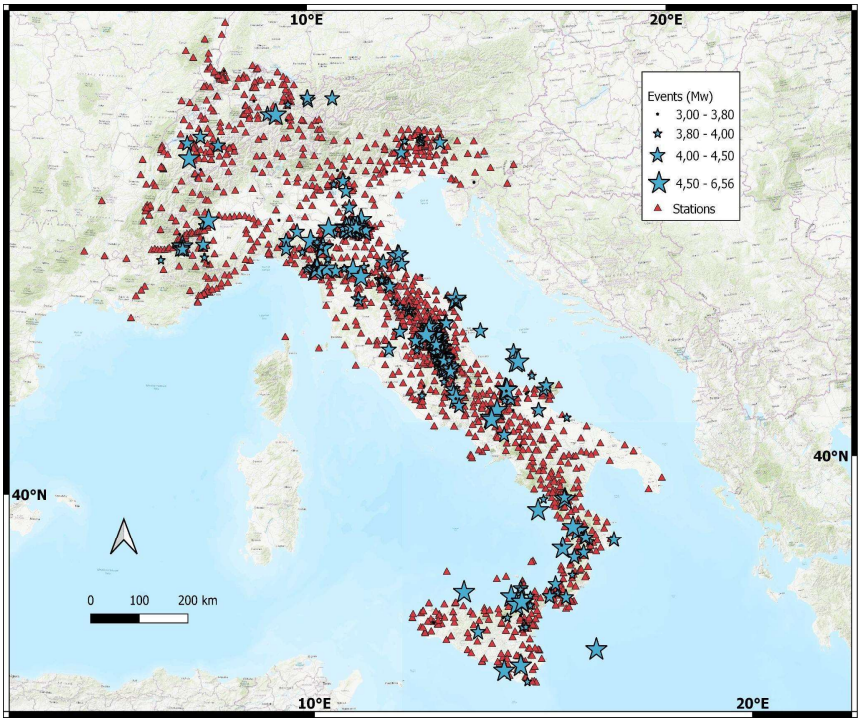

Figure 1. Map of Italian events and stations in the calibration dataset

In order to correctly interpret the results of the residual analysis discussed in the next section, we homogenize the moment magnitudes M_w of the events. In particular, the M_w calculated with the TDMT method (Time Domain Moment Tensor; Dreger, 2003), are converted into M_w estimated with the RCMT method (Regional Centroid Moment Tensor; Pondrelli, 2002), because in the assumed reference GMM, the explanatory variable for magnitude scaling is the RCMT. For this purpose, we adopt a conversion law calibrated by Brunelli et al (2022b) based on 141 events, for which both the M_w

estimates from TDMT, available from the INGV web-service (http://webservices.ingv.it/), and the M_w estimate with the RCMT method, extracted from the European-Mediterranean RCMT Catalog (https://rcmt2.bo.ingv.it/), are available. This conversion ensures a reduction of the between-event variability due to inhomogeneous magnitude estimates.

Fig. 2 displays the number of records per event in the dataset, which shows that in the majority of the events, more than 60 waveforms are recorded. The Figure also shows the magnitude M_w-RCMT (hereinafter only M_w) vs distance distribution; the latter is represented by the Joyner-Boore distance when the fault geometry is available (for all the events with M_w>5.5), otherwise the epicentral distance is considered.

The flat-file of this dataset is available online (see "**Data Availability**" section), and is formatted consistently with the Engineering Strong Motion (ESM) flat-file (Lanzano et al. 2018). It comprises observed ground motion parameters provided by the ITACA database including PGA and SA at 27 spectral periods that extends up to 4s.

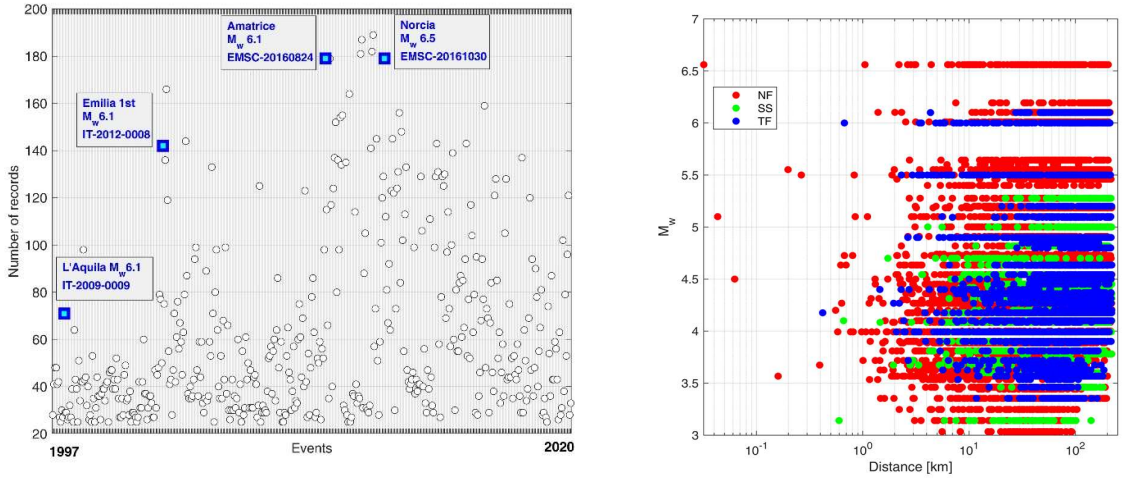

Figure 2. a) number of records per event (the largest events occurred in Italy are marked); b) magnitude-distance scatter plot according to different focal mechanisms (NF - Normal Fault; SS - Strike Slip; TF - Thrust Fault).

3. Ground motion model

On the above dataset, we investigate the spatial features of the Italian ground motion based on a residual analysis (Al-Atik et al., 2010). In detail, we compute the total residuals R_{es} of a given GMM, as the logarithm difference between the observed ground motion IM (log10-units), i.e. $\log(IM)_{obs}$ and the corresponding prediction $\log(IM)_{pred}$ obtained from the reference GMM. The reason for such an approach is that the residuals, by definition, take into account the unmodelled

effects (i.e. the unaccounted covariates in the model description) that show a spatial dependence. Therefore, through the residuals, it is possible to trace the spatial correlation structure and reconstruct the pattern of ground shaking.

Here we adopt as GMM the model by Bindi et al. (2011), whose acronym is ITA10, which predicts spectral IMs, as the Peak Ground Acceleration (PGA), Peak Ground Velocity and acceleration response spectra SA (damped at 5%) in the interval 0.01-2s. It is valid for active crustal regions in the magnitude range 4.0-6.9.

Despite the availability of a more updated GMM for Italy (i.e. the ITA18, Lanzano et al., 2019), we selected the ITA10 as a reference model for the analyses because it is the longest implemented within the mostly used tools for hazard assessment (OpenQuake, Pagani et al., 2014) and engineering applications (the Italian Shakemap, Michelini et al, 2020). However, although the spatial correlation depends upon the adopted GMM (Schiappapietra and Douglas, 2020), we do not expect significant variations with respect to the most recent model, as the ITA10 and ITA18 produce similar predictions being calibrated on earthquake data that are the expression of the same tectonic setting and geological/crustal conditions of Italy.

The ITA10 functional form is synthetically recalled in the following:

$$log_{10}Y_{es} = log_{10}\overline{Y}_{es}(M_w, R, S, SOF) + \eta'_e + \varepsilon'_{es} \qquad [1]$$

where Y_{es} is the intensity measure to regress at s^{th} site due to the e^{th} event. $\overline{Y}_{es}$ is the median prediction of the model expressed as a function of several explanatory variables (i.e. the moment magnitude M_w, the source to site distance R equal to the Joyner–Boore distance or the epicentral distance when the fault geometry is unknown, the site S and the style of faulting SOF).

In Eq. [1], the median prediction $\overline{Y}_{es}$ for ITA10 is schematically expressed as follows:

$$log_{10}\overline{Y}_{es} = a + F_D(R, M_w) + F_M(M_w) + F_S + F_{SOF} \qquad [2]$$

where a is a constant term, $F_D(R, M_w)$ is a distance function including a term linearly decreasing with distance (anelastic attenuation), $F_M(M_w)$ is a bi-linear magnitude scaling, F_S the site amplification linearly depending on dummy variables used to denote the five different Eurocode 8 (CEN 2004) site classes, and F_{SOF} the style of faulting correction that is modeled with dummy variables to denote the different fault classes. For more details on the model, the reader can refer to Bindi et al. (2011).

178 The total residuals $R_{es} = \eta'_e + \varepsilon'_{es}$ are random-effects of the regression (Stafford, 2014; Bates, 2015) according to the
179 approach and notation of Al-Atik et al. (2010). Namely, $\eta'_e \sim \mathbb{N}(0, \tau')$ are zero-mean (Gaussian) normally distributed
180 between-event residuals with standard deviation τ'. They represent the systematic deviation observed between prediction
181 and observation for a specific event *e*, i.e. the mean of the residuals for a specific event. Several authors have shown that
182 η'_e are correlated with some source characteristics not captured by the standard magnitude scaling in GMMs (e.g. stress
183 drop or focal depth, see Bindi et al., 2017). More in general, it depends on the geometric variations in the faulting
184 properties or the dynamic rupture process, which are common to different sites (Jayaram and Baker, 2007); thus it is
185 usually not included in spatial correlation modeling.
186 The terms $\varepsilon'_{es} \sim \mathbb{N}(0, \phi')$ are zero-mean (Gaussian) within-event residuals with standard deviation ϕ', describing the
187 average misfit of ground-motion at the site with respect to the event-corrected median value predicted by the GMM. They
188 include regional propagation features or effects that are not captured by the general model, such as slip patches of the
189 rupture and directivity effects (Colavitti et al. 2022), in addition to missing covariates depending on the surface geology,
190 which are not fully explained by the site proxy introduced in the functional form (i.e. the EC8 site class for ITA10).
191 Depending on site effects, the within-event component reflects spatial variability of ground-motion from one site to
192 another and thus it is generally used to model the spatial correlation.
193 In the following, we consider the residuals ε_{es} which are dimensionless data points normalised to their standard deviation:

194 $$\varepsilon_{es} = \frac{\varepsilon'_{es}}{\phi'} \qquad [3]$$

195 ε_{es} follow a multivariate Gaussian distribution with unitary standard deviation $\phi = 1$; they are completely defined by the
196 mean and covariance function, which reflects the correlation of within-event residuals (Schiappapietra and Douglas,
197 2020).
198 We visually inspect the spatial distributions of ε_{es} to identify potential patterns over the Italian domain. Some examples
199 are reported in Fig. 3 where the bubble plots of the normalized residuals exhibit some spatial trend.
200

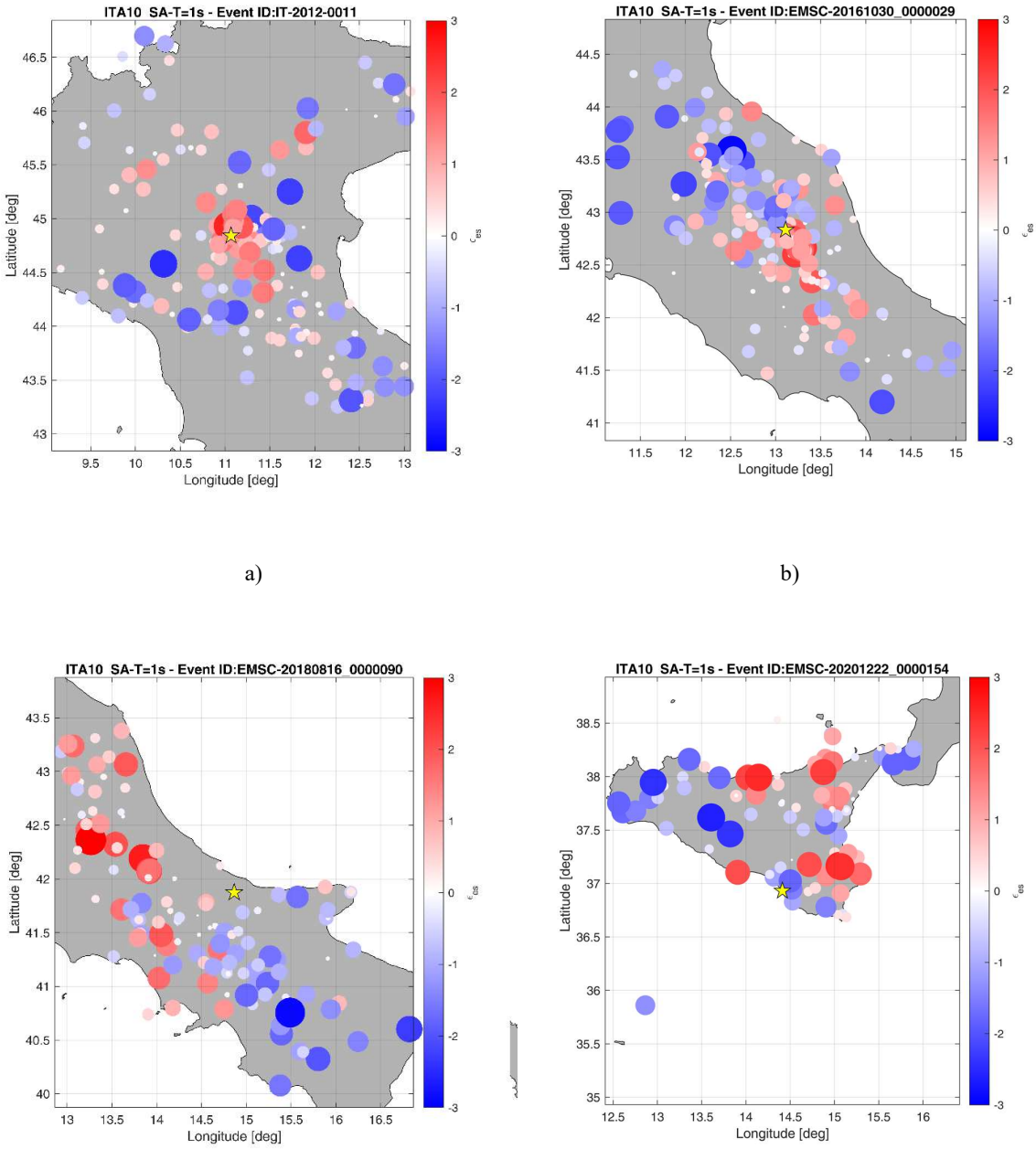

Figure 3. Bubble plot of the normalised residuals at PGA for example events in the dataset: a) 2012.05.29 in Northern Italy (ESM code: IT-2012-0011); b) 2016.10.30 in Central Italy (ESM code: EMSC-20161030_0000029); c) 2018.08.16 in Southern Italy (ESM code: EMSC-20180816_0000090); 2020.12.22 in Sicily (ESM code: EMSC-20201222_0000154). Colors are coded according to the sign of the residuals: positive values are red-colored whereas negative values are blue-colored.

4. Method

To estimate correlation, the data ε_{es} are considered spatially-varying random variables representing local fluctuations of each event with respect to a baseline averaging ground motion effects over space. On these residuals, the hypothesis of second-order stationarity and isotropy is usually made due to the lack of repeated ground motion observations from the same event at a given site (Schiappapietra and Douglas, 2021); under these hypothesis we assume that the mean function of the random variable ε_{es} is constant for all sites and the correlation depends only on the separation distance (h) between two sites *i* and *j* and not on their absolute location (i.e. $[\rho(\varepsilon_{es,i}, \varepsilon_{es,j}) = \rho(\mathrm{h})]$.

Hence, we can get the correlation structure in a simplified manner, that is by calculating experimental semivariograms $\gamma(h)$ on ε_{es} to measure the average dissimilarity between spatially distributed data, as done by many authors e.g. Jayaram and Baker, (2009); Oliver and Webster (2014); Schiappapietra and Douglas (2020). To do this, we use the classic estimator based on the method of moments (Matheron 1962), as follows:

$$\gamma(h) = \frac{1}{2} E\left[\left(\varepsilon_{es,i} - \varepsilon_{es,j}\right)^2\right] \quad [4]$$

where the mathematical operator $E[\ ]$ denotes the expected value. The empirical estimation of $\gamma(h)$ from the observed residuals can be done via the following equation:

$$\hat{\gamma}(h) = \frac{1}{2N(h)} \sum_{D_{i,j}=h} \left[\left(\varepsilon_{es,i} - \varepsilon_{es,j}\right)^2\right] \quad [5]$$

being $D_{i,j}$ the inter-site distance between site i and site j which is assumed equal to h within a given tolerance ($\left|D_{i,j} - h\right| \leq \Delta h$), where the tolerance Δh is the bin distance, whereas $N(h)$ is the number of observed station pairs with separation distance h.

In this work, we performed some trials to set a bin size appropriate to obtain stable semivariograms and enough populated bins, then we chose a compromise value of 12 bins with equal width of 8 km. The maximum considered distance when computing semivariograms is 100 km, which is half of the maximum distance of validity of the GMM (i.e. 200 km). In this way, a high number of site pairs is sampled on average as shown in Fig. 4.

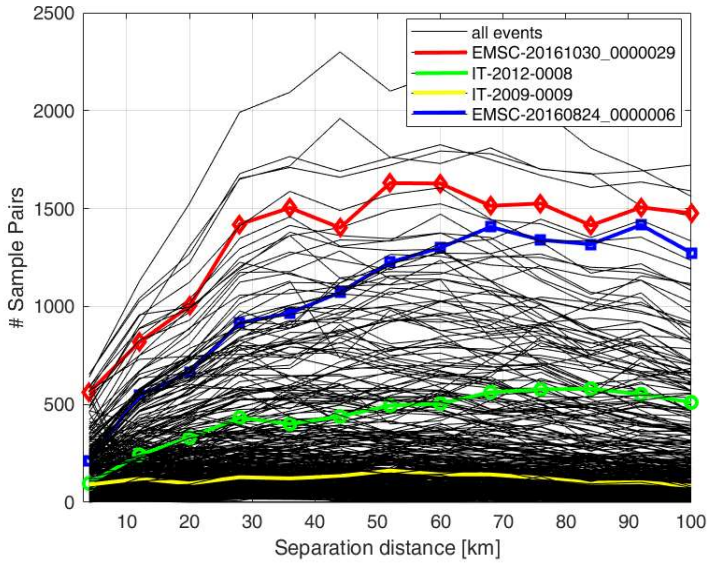

Figure 4. Number of data pairs as a function of site-to-site separation distance bin (8 km). Marked lines correspond to the largest Italian earthquakes in the dataset.

An increasing trend versus separation distances h usually characterizes sample semivariograms up to a given correlation length after which no more spatial correlation is observed; then it stabilizes asymptotically at the level of data variance. The first analysis of the sample semivariograms of our data reveals some non-stationarities identified by unstable plateaus (i.e. increasing trend with separation distance increasing that determines overestimated correlations), which is somewhat expected, since we are looking at data from a wide geographic domain, implying the need to go beyond the assumption of stationarity. Assuming non-stationarity means that there is a mean spatial trend underlying the data, due to systematic unmodelled effects typical of the ergodic ground motion models. In this case, the expected value of the random variable E[ε_{es}] may not be constant across all sites, but indeed varying depending on the location (Schiappapietra and Douglas, 2020).

In order to manage non-stationarity and remove the observed deterministic component of spatial variability from each data point (i.e. the residuals ε_{es}), we first try to adopt usual detrending technique based on the use of a polynomial surface fitting dependent on the geographic coordinates (Oliver and Webster, 2014; Sgobba et al., 2021) on which however, we experienced instability in the local curvature at the boundary of the surface, where the constraint to data is weaker. To overcome this drawback, we use the Inverse Distance Weighting (IDW) algorithm (Chen and Liu, 2012) to interpolate the ε_{es} residuals to create a trend surface. Assuming to have *n* residuals we perform *n* interpolations leaving one point out

each time. The residual corrected for the trend is the difference between the original ε_{es} value and the value of the trend surface at that particular point. This allows to obtain more robust results in terms of the stability of the semivariograms of the reminaing residuals (i.e. the residuals purifies of the deterministic average trend). The removed component, called *drift*, is plotted in Fig. 5 by stations as a function of distance and with varying spectral periods. It can be seen that there is a bias at longer distances (above 80 km about) that is more significant at short periods. This may represent an adjustment to ITA10; indeed, anelastic attenuation is not properly described by ITA10 as highlighted by previous studies (Zimmaro et al., 2018, Lanzano et al., 2019 and reference therein), resulting in a residual bias at short periods and long distances. Indeed, the effects of the anelastic attenuations become relevant for long event-station distances (Sedaghati & Pezeshk, 2017).

In the following, we will refer to the de-trended results (i.e. after *drift* removal) as the "non-stationary case" and to the estimates as-they-are (i.e. without de-trending) as the "stationary case".

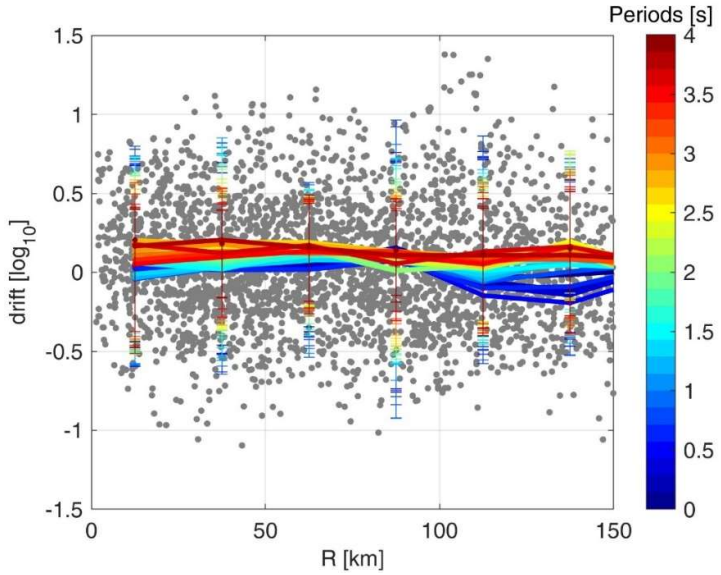

Figure 5 Mean drift by station with error bar (solid lines) versus distance R colored according to different spectral periods.

4.1 Univariate spatial analysis

Under (second-order) stationarity and isotropy assumption, we can assume that the semivariogram and the covariance function are equivalent (Oliver and Webster, 2014). This means that we can adopt a common semivariogram fitting function to model the correlation structure. In doing this, we implement an automatic fitting algorithm due to the large number of earthquakes and the number of periods to be analysed, similar to Loth and Baker (2013). Namely, we adopt

the exponential relationship, which is the most used functional form in seismology (Schiappapietra and Smerzini, 2021) that is defined as:

$$\hat{\gamma}(h) = sill \left[1 - \exp\left(\frac{-3h}{range}\right)\right] \quad [6]$$

where the $sill$ is the semi-variance of the residuals and represents the asymptotic value of $\hat{\gamma}(h)$ for $h \to \infty$, whereas the $range$ is defined as the value of the separation distance h corresponding to the 95% of $\hat{\gamma}(h)$ that represents the maximum separation distance above which two sites are spatially uncorrelated. In the present case, the $sill$ value is equal to 1, due to previous normalization of the residuals ε_{es} and we also assume that there is no *nugget* effect (i.e. we consider neglecting the small-scale errors).

Hence, the unique unknown parameter is the $range$, which is the searched correlation distance to determine for characterizing the spatial correlation structure of our data. Its estimate largely depends on the adopted fitting technique (Schiappapietra and Douglas, 2020), and specifically on the metric used to evaluate the misfit. Indeed, there is no general consensus on the most appropriate method to apply on seismological data, therefore, to achieve robust estimate of $range$ values, we test different techniques applied to our residuals, to find the best fitting model; namely we adopt the same algorithms examined by Baker and Chen (2020): i.e. i) the Ordinary Least Squares (OLS), which minimizes the sum of squared differences between the data and the model (i.e. the error); ii) the Weighted Least Squares (WLS1) incorporating weights on the squared errors that tend to apply larger weights to small-distance values (smaller h) and more populated bins (larger $n(h)$), as follows:

$$w = n(h)e^{-\frac{h}{c}} \quad [7]$$

being w the weight, n the number of separation distances, c is a factor controlling the rate of weight decreasing with h increasing (fixed to 5 km, according to Baker and Chen, 2020 and verified as appropriate after preliminary tests); iii) the Weighted Least Squares (WLS2) defined as point ii) but incorporating weights as:

$$w = \frac{n(h)}{h^2} \quad [8]$$

iv) the Linear Regression transformation LR (Loth and Baker, 2013). More details on the methods can be found in Baker and Chen (2020).

A comparative plot of the mean error across all earthquakes and associated with each fitting method (i.e. the squared differences between the observed semivariogram data and the fitted function, weighted according to the specific fitting technique, as in Baker and Chen, 2020) is shown in Figure **ESUPP1** in the supplementary material. These results indicate that the weighted least squares (WSL) fitting methods perform better than the alternatives, as noted by Baker and Chen (2020). In our analysis, WSL1 and WSL2 provide essentially the same performance, so we deemed it irrelevant to use either of the two weighting method, thus in the following we continue to consider the earthquake-specific semivariograms fitted with the WLS1.

Fig. 6 shows some semi-variogram examples fitted with the four above techniques along with the empirical data.

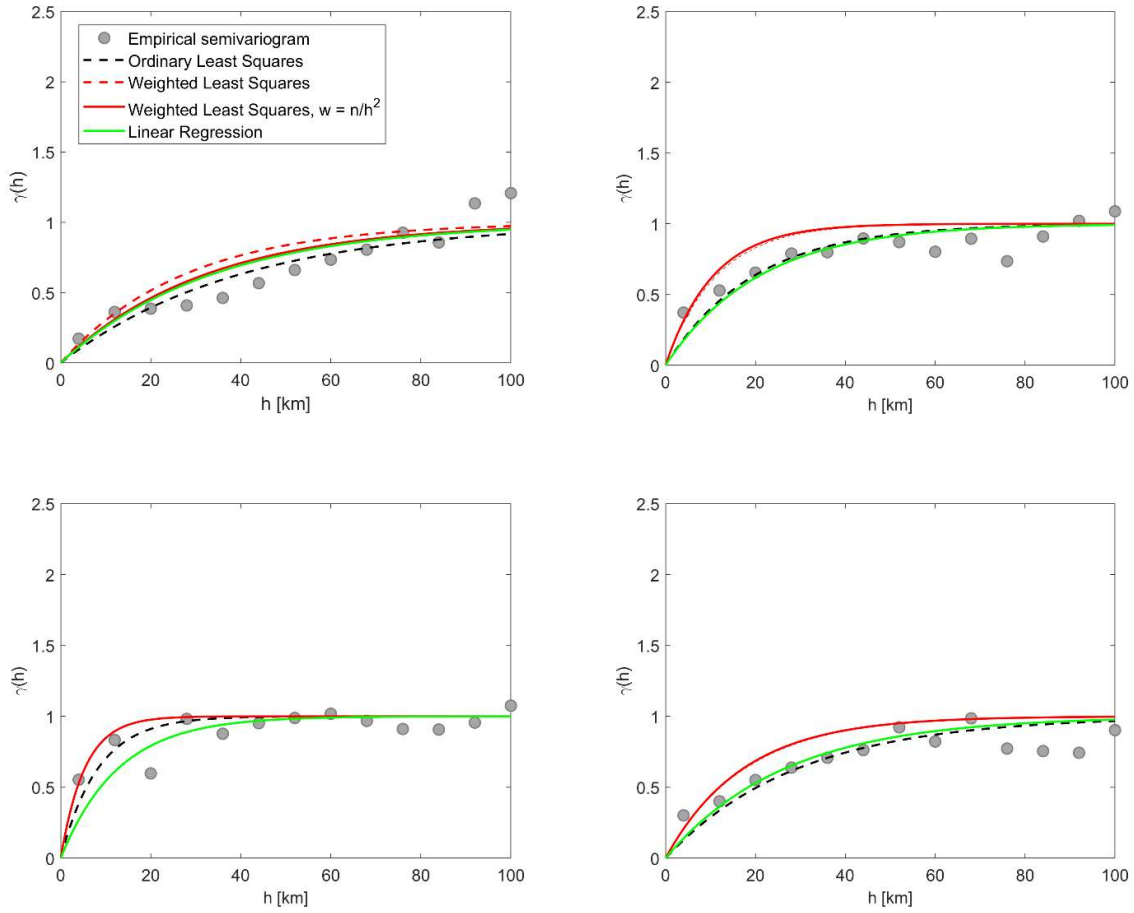

Figure 6. Example of empirical (non-stationary case) semivariograms and fitting functions for SA(3s): a) 2012.05.29 in Northern Italy (ESM code: IT-2012-0011); b) 2016.10.30 in Central Italy (ESM code: EMSC-20161030_0000029); c) 2018.08.16 in Southern Italy (ESM code: EMSC-20180816_0000090); 2020.12.22 in Sicily (ESM code: EMSC-20201222_0000154).

5. Results

The average of *range* values calculated for each individual event are plotted against periods in Fig. 7 (the *range* estimates are provided in the table **ESUPP2** in the supplementary material), along with the predictions by the global models of Jayaram and Baker (2009) and Heresi and Miranda (2019), as well as with Huang and Galasso (2019) and Esposito and Iervolino (2012), who calibrated spatial correlation models specifically on Italian datasets.

Note that, instead of applying an arithmetic average to the *range* values, we opt for a weighted average in which the weight assigned is equal to the inverse of the number of records associated with each event. In this way, smaller weights are given to events that are less sampled in the dataset and for which the uncertainty in estimating the *range* parameter is greater, as also described by Baker and Chen (2020) and Schiappapietra and Douglas (2020) who demonstrated that the correlation estimation uncertainty is inversely correlated to the number of available stations.

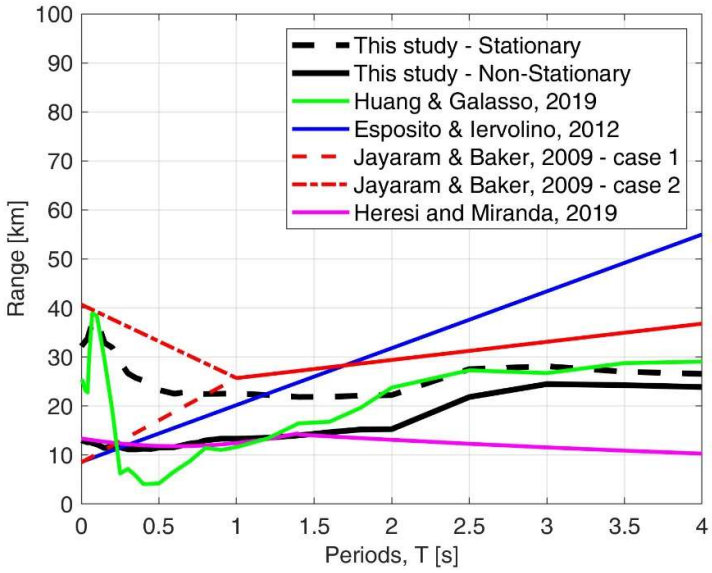

Figure 7. Average *range* provided in this study for Italy (black lines) versus periods compared with literature models.

Fig. 7shows that higher values characterize the main trend in the stationary case (i.e. without removing the *drift*) at very short periods (T<0.2s); then, it decreases slightly up to about 2s to increase again with the period increasing. The latter trend for long-periods is common to nearly all the considered models and in line with past studies since the coherency in amplitude and phase angle between the frequency components of seismic waveforms increases with period increasing (Zerva and Zervas, 2002). The stationary case is intermediate to the models proposed by Jayaram and Baker (2009), in that we expect that there are some regions in Italy that show heterogeneous geologic site conditions (model case 1) as in Central Italy, and others that show site clustering conditions (model case 2), as in the Po Plain.

335 The observed trend is also consistent with the model of Huang and Galasso (2019) (hereinafter recalled as HG) and with
336 a similar peak at T<0.2s, despite the adoption of a different method to get spatial correlation parameters (i.e. a one-stage
337 nonlinear regression algorithm) calibrated on an ITACA dataset composed by 233 events and 7843 records (version
338 updated to 2018) similar to that adopted in this study.
339 The estimates differ from that of Esposito and Iervolino (2012) (hereinafter recalled as EI) even if these authors used a
340 similar geostatistical approach and the same GMM (ITA10) considered in our study. We attribute such differences to the
341 diversity in the calibration dataset; in fact, EI employed 763 records from 97 events in ITACA that are almost the same
342 as used to fit the ITA10 model, thus obtaining smaller residuals that lead to less correlation. In contrast, our dataset
343 contains a large amount of smaller events, introducing larger variability in the short-period range. This effect is removed
344 when passing to the non-stationary model (i.e. with *drift* removal), which then produces estimates more similar to those
345 by EI at short periods. The non-stationary case shows a more stable trend in the short periods and lower values over
346 almost the entire range of periods.
347 In general, the observed differences in the models are more marked at short periods, where the reference GMM and the
348 dataset used to compute the residuals seem to play a crucial role in estimating of the correlation distance, as also
349 highlighted by Schiappapietra et al. (2022). This behavior may depend on the different ability of the GMMs to capture
350 the anelastic attenuation. Conversely, at intermediate and long periods, the models converge towards a more similar trend.
351 *Ranges* patterns are plotted in Fig. 8 for individual earthquakes, showing that the variability associated with the estimates
352 is relatively large, likely due to highly heterogeneous geological/geomorphological settings that feature the Italian
353 territory. Here we report the results for the stationary case, as they are not affected by the *drift* estimation, in order to
354 better compare them with the results of previous works. For example, the events Mw6.5 Norcia EMSC-20161030_000029
355 and Mw6.1 Amatrice (EMSC-20160824_000006), both recorded in central Italy (CI), are characterised by relatively
356 lower *range* values, in line with the studies by Schiappapietra and Smerzini (2021) and Schiappapietra et al. (2022) for
357 the CI. Instead, the Mw6. 1 of Emilia 2012 (IT-2012-0011) is characterised by larger estimates at longer periods due to
358 basin effects in the Po Plain, in agreement with the results of Infantino et al. (2021), Sgobba et al. (2019) and
359 Schiappapietra et al. (2022) for Northern Italy (NI). In Southern Italy (SI), the results are highly variable, as lower *range*
360 are observed, such as in western Sicily (EMSC-20200923_0000176) and Molise (EMSC-20180816_0000090), in
361 agreement with Schiappapietra et al. (2022) for SI, while we observe larger values for events in south-eastern Sicily,
362 which are enucleated in a carbonate foreland, e.g. Mw4.2 EMSC-20160208_0000065 (Hyblean plateau).
363 A further observation concerns the main trend of the event-specific curves in Fig. 8, where one can note a more variable
364 behavior at short periods and more stability for periods T>1s. In addition, the long-period part of these curves seem to be

365 more consistent with the expected physical trend of correlation (e.g. Emilia IT-2012-0011 shows larger ranges at long T,

366 as expected in the Po Plain region).

367

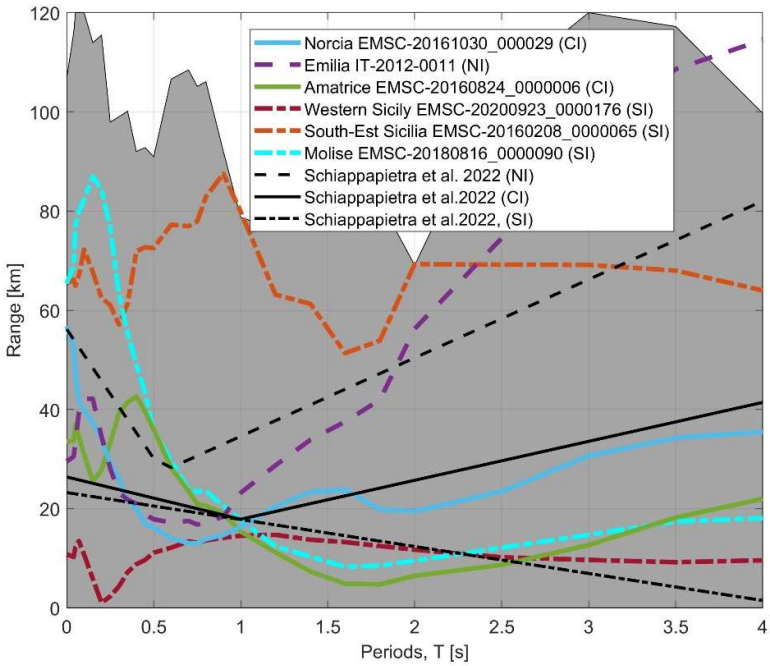

368

369 **Figure 8.** *Range* estimates vs periods for some specific events in the dataset dinstinct for area (NI: Northern Italy; CI:

370 Central Italy; SI: Southern Italy). The shaded gray area indicates the total variability of the *range* estimates in the dataset.

371

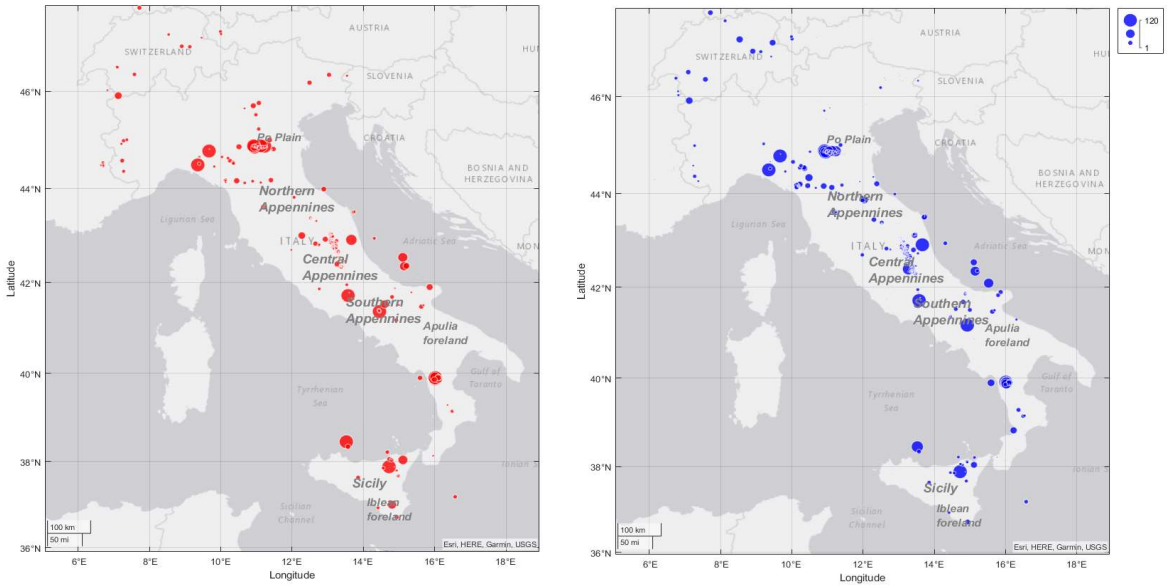

Figure 9. Mean *range* estimates (non-stationary) on the Italy map for short (left) and long periods (right).

We guess that the event-specific differences observed in the *range* values, reflect some regional features related to the seismic propagation through the crust combined with large-scale site amplifications/deamplification and anisotropic ground motion effects near the source rupture. Hence, the latter aspects represent unmodeled effects included in the within-event residuals, whereas the amount of variability linked to the individual event and tectonic features are mainly removed with the between-event components. To explore these aspects and evaluate the spatial distribution of the correlation structure over Italy, we plot on map the *range* values (Fig. 9) to identify potential spatial patterns. The map shows a high variability across different regions that may indicate some physical effect underlying the observed variability, such as spatial anisotropy in the anelastic attenuation. For example, larger correlation lengths both at short and long periods are focused in the areas of the Apulian carbonate platform (the northern part) and the Eastern Sicily (Iblean plateau), marked by bigger bubbles, which are also characterized by slower attenuation properties of ground motion (Brunelli et al., 2022b). Higher correlation is also noticeable in the area of the Po Plain where resonance and amplification effects occurring at sites within and at the borders of the basin tend to produce highly correlated ground motions (Sgobba et al., 2019; Menafoglio et al., 2020).

These main findings corroborate the hypothesized link between the level of correlation and attenuation/site properties, even if a univocal physical interpretation is difficult to draw and it is out of the scope of the present study.

5.1 Adaptation of the Loth and Baker (2013) model

As the main aim of this study is to calibrate a spatial correlation model for Italy for application in the Italian Shakemap, we compare our results with those implemented within that tool in the default configuration, i.e. the Loth and Baker's model (Loth and Baker, 2013 corrected after Loth and Baker, 2020, hereinafter referred to LB13).

LB13 is a global spatial model valid for crustal earthquakes in active seismic regions, calibrated on 8 well-sampled earthquakes that occurred in Japan, California and Taiwan.

In that study, the authors formulate a spatial cross-correlation model of spectral accelerations by which they generalize the modeling to a multivariate framework to account simultaneously for spatial and spectral correlation (i.e. the cross-correlation between spectral ordinates at different periods).

They make a fundamental assumption based on the stationary hypothesis, that is, the spatial covariance C is directly related to the semivariogram function γ as follows:

$$C(h) = C(0) - \gamma(h) \qquad [9]$$

where $C[\,]$ is the covariance operator and $C(0) = \phi^2$ that is the variance of the random variable Z (in this case the residuals ε_{es} have unitary variance $\phi^2 = 1$ due to the previous normalization of Eq. [3]).

LB13 extend Eq. [8] to the multivariate case, by defining the isotropic semivariogram matrix $\boldsymbol{\Gamma}(h) = \left[\gamma_{ij}(h)\right]$ and the isotropic full covariance matrix $\boldsymbol{C}(h) = \left[C_{ij}(h)\right]$ for two random variables $\varepsilon_{\boldsymbol{es},i}(T_1)$ and $\varepsilon_{\boldsymbol{es},j}(T_2)$ (e.g. the normalized residuals of the spectral ordinates at two periods respectively T_1 and T_2 and at spatially separated locations i and j distant h), so that the relation [9] is generalized as follows:

$$\boldsymbol{C}(h) = \boldsymbol{C}(0) - \boldsymbol{\Gamma}(h) \qquad [10]$$

To solve Eq. [10] for the multivariate case, however, the matrix $\boldsymbol{C}(h)$ must be positive definite as in the univariate case (i.e. the variances of the variables ε_{es} defined at a certain number of sites and periods, must be non-negative). However, using the approach before described and thus fitting each empirical semivariogram independently takes no such constraint into account when estimating the *range*, therefore not necessarily leading to a positive definite covariance matrix.

To overcome this drawback, LB13 invoke the so-called "separation model" (Banerjee et al., 2004) so that the covariance matrix of Eq. [10] can be rewritten by Eq. [11]:

$$\boldsymbol{C}(h) = \rho(h) \cdot \boldsymbol{C}(0) \quad [11]$$

where $\rho(h)$ is a scalar function named correlation coefficient, which is related to the semivariogram by:

$$\rho(h) = 1 - \frac{\gamma(h)}{\phi^2} = \exp\left(\frac{-3}{range}\right) \quad [12].$$

Using this approach, the problem of solving the full covariance matrix positive definite reduces to the need to have a positive definite covariance matrix at the single site $C(0)$, being the latter defined only for the number of considered periods and not also for the number of sites.

Yet, it is not possible to fit a single range of Eq. [12] to be adopted in Eq. [11] for the whole model as it does not reflect the real correlation features in the data at different scales. LB13 solves this problem with a linear model of co-regionalization that is equivalent to model each variogram and cross-variogram. A complete mathematical description is provided in Loth and Baker (2013); here, we limit to point out that they make an extension of the separable model to incorporate multiple *range*, which is called linear model of co-regionalization:

$$\boldsymbol{\Gamma}(h) = \sum_{l=0}^{L} B^l \gamma^l(h) \quad [13]$$

The latter assumes that the semivariogram matrix of all the random variables is a linear combination of some basic semivariogram functions $\gamma^l(h)$ chosen *a-priori* to represent the spatial structure at different scales, B^l are the coregionalization matrices and L is the number of the independent underlying structural components. This number is equal to 3 in LB13, in order to minimize the number of structures and simplify both calculation and interpretation (Loth and Baker, 2013), so that the identified correlation functions $\gamma^l(h)$ are: i) a short range acting on small-periods, ii) a large range acting on long-periods and a iii) nugget effect for very short-periods, which is assumed constant.

As a result, combining Eq. [12] and [13], LB13 model is simplified as follows:

$$\boldsymbol{\Gamma}(h) = B^1\left(1 - \exp\left(\frac{-3h}{r_1}\right)\right) + B^2\left(1 - \exp\left(\frac{-3h}{r_2}\right)\right) + B^3 \quad [14]$$

In Eq. [14], it can be noted that the identified *range* values of the exponential model $r1$ and $r2$ are equal to 20 km and 70 km, respectively for the short- and long- period. These two values proved to be adequate in describing the spatial correlation structure of observed ground motion in LB13; however, since spatial correlation is also region-dependent

(Schiappapietra and Douglas, 2020); here, we propose different correlation lengths for the Italian context. Hence, we only modify the range values while maintaining the same co-regionalization matrices B^1, B^2 and B^3 of Eq. [13], as we assume that the spatial and spectral parts of the cross-correlation matrix are independent of each other because of the separation model (Eq. [11]).

The candidate range for Italy are r1=13 km and r2=25 km, chosen as short-range and long-range values and respectively implemented in the two exponential basis functions of LB13 coregionalization model (Eq. [14]). These values were preliminarily selected in light of the previous univariate analysis, considering the maximum values assumed in the weighted average trend of the *range* distances (non-stationary case) for short (T<1s) and long (T>=1) periods. Then, the candidate values were confirmed on the basis of the best-fit outcome of the direct and cross-semivariograms of the most sampled earthquakes, thus extending to the multivariate case. We do not include the nugget among the parameters of the new model, as we guarantee the fit at small separation distances provided by the LB13 co-regionalisation model. We perform the fitting on the empirical semivariograms derived from the non-stationary analysis because this approach allows us to remove the deterministic component (i.e. the *drift*) and is therefore best suited to provide a better resolution of the multiscale variability of our spatial data. Indeed, the *drift* represents a large-scale model, while the remaining random component can be modelled as a second-order stationary process containing short- and long-range effects.

In Fig. 10 we show some examples of how the LB13, modified with r1 and r2 intervals for Italy, fit the empirical semivariograms in comparison with the original LB13. The events considered are among the best sampled ones in different regions of Italy and previously shown with reference to the univariate analysis, i.e. i) event 2012.05.29 in Northern Italy (IT-2012-0011) with 166 records; ii) event 2016.10.30 in Central Italy (EMSC-20161030_0000029) with 179 records; iii) event 2018.08.16 in Southern Italy (EMSC-20180816_0000090) with 128 records and iv) event 2020.12.22 in Sicily (EMSC-20201222_0000154) with 60 records. The curves provide a good fit on both direct and cross-semivariograms, from which we can infer the adequacy of the adopted functional form and *range* distances.

As already mentioned, in this study we intend to modify the LB13 model only for the correlation distance while adopting the same coregionalisation matrices calibrated by LB13. Indeed, we assume the separability of the covariance function, as already done by other authors, such as LB13 and Goda and Hong (2008), according to whom spatial and spectral structures can be modelled separately.

To get an idea of the adequacy of the coregionalization matrices to our data, we evaluate the median predictions of LB13 at zero-distance (i.e., the cross-correlation matrix obtained from Eq. [14] for h = 0) in order to account only for the spectral part. The results for each IM are shown in Fig. 11, where the semi-variogram residuals (i.e., the difference between the

empirical data and the prediction of LB13 at zero distance) are compared. The correspondence is acceptable, especially for longer periods, so we ignore the spectral part in our analysis.

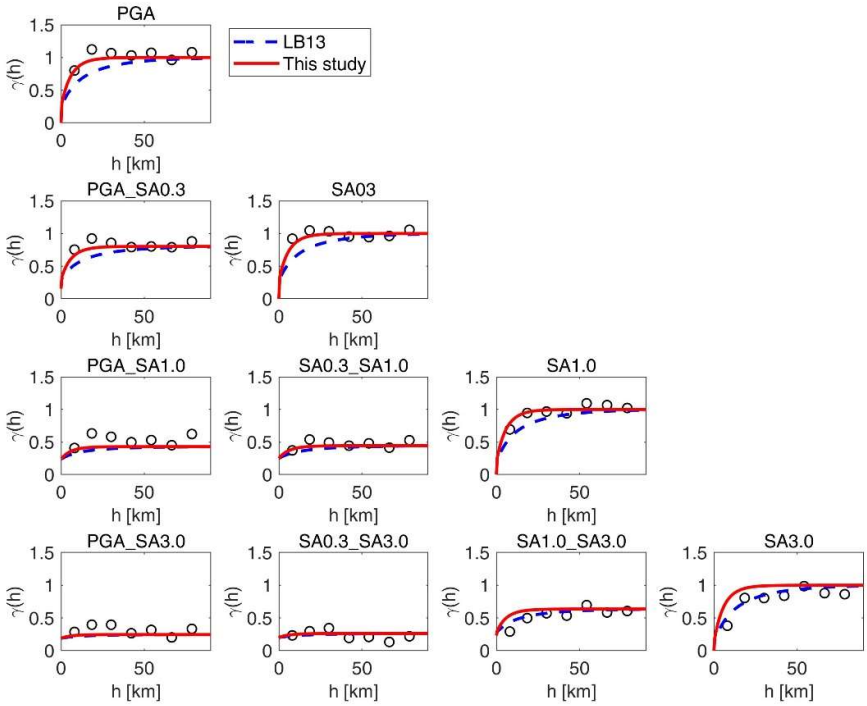

a)

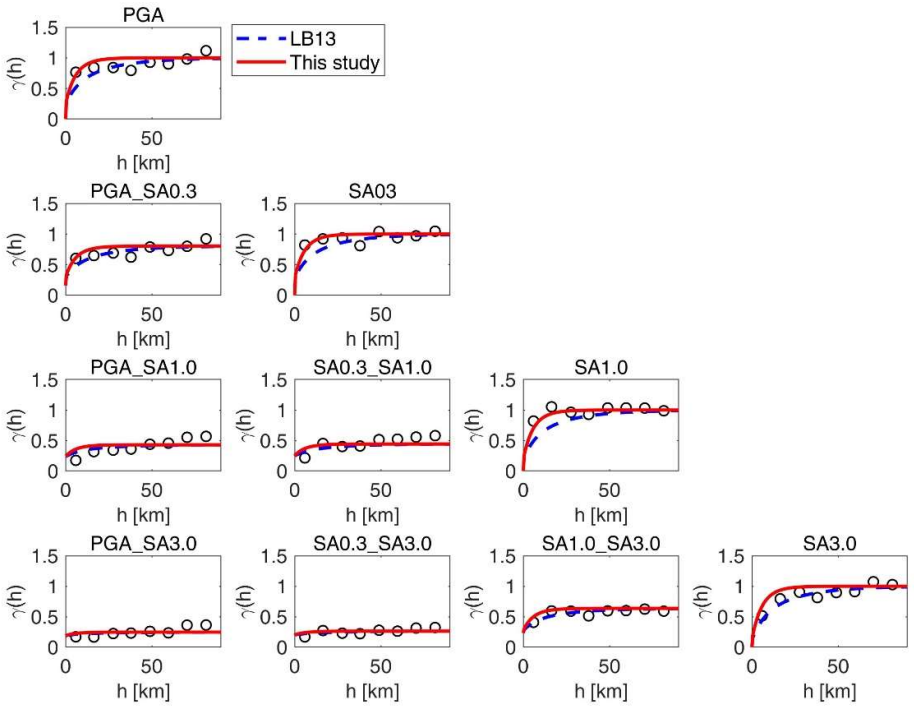

484

485 b)

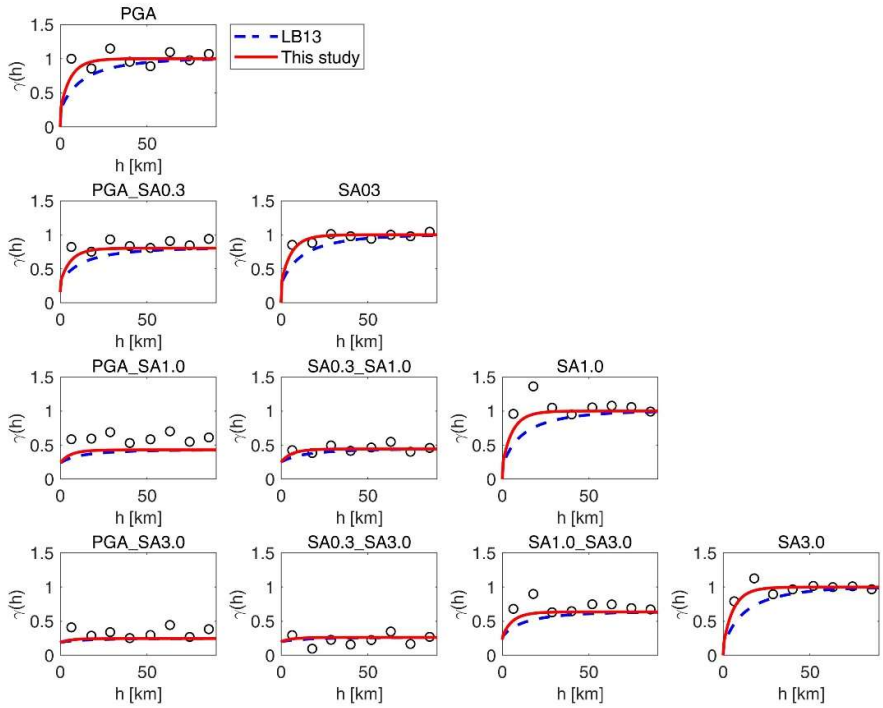

486

487 c)

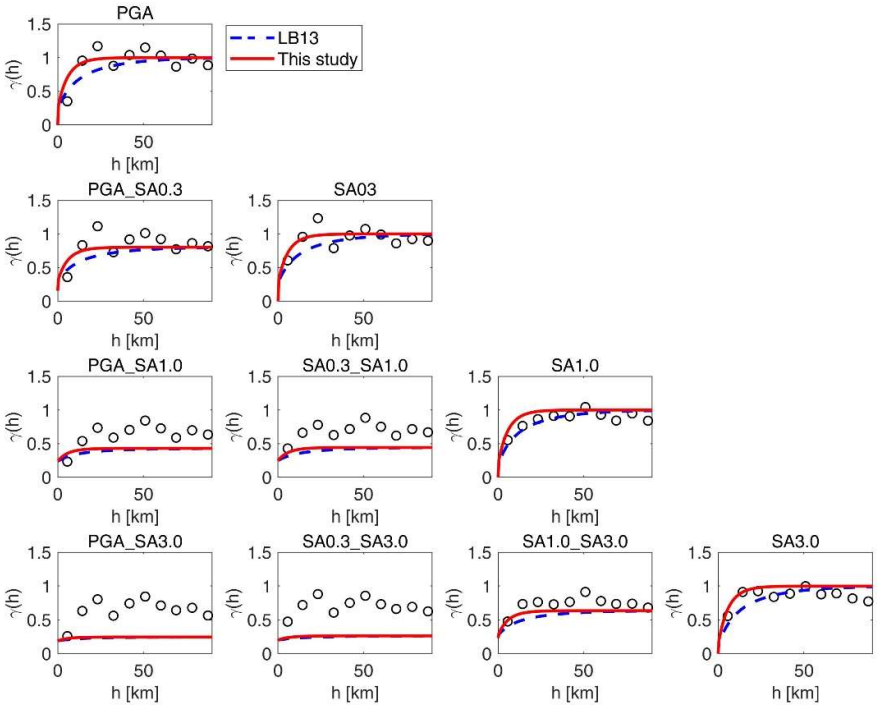

d)

Figure 10. Sample (circles) and modeled (curves) semi-variograms of earthquakes: a) 2012.05.29 in Northern Italy (ESM code: IT-2012-0011); b) 2016.10.30 in Central Italy (ESM code: EMSC-20161030_0000029); c) 2018.08.16 in Southern Italy (ESM code: EMSC-20180816_0000090); d) 2020.12.22 in Sicily (ESM code: EMSC-20201222_0000154).

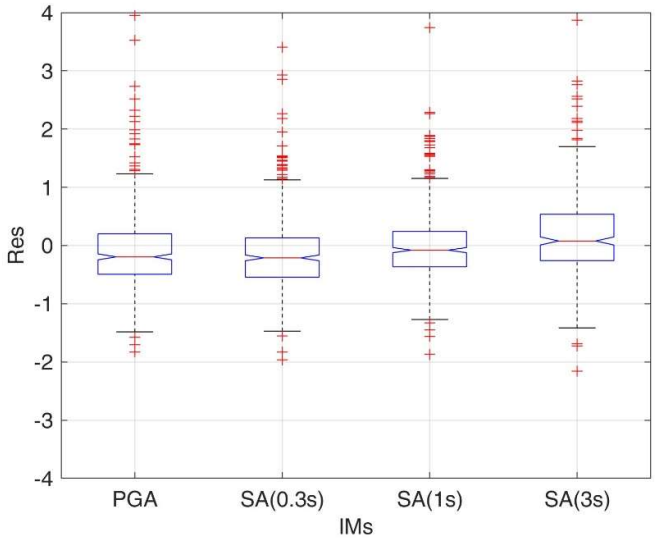

Figure 11. Boxplot of the residuals (Res) of LB13 at zero distance for different IMs.

6. Validation

In this section, we quantify the effects of the new spatial correlation model within the Italian configuration of ShakeMap. As already applied to test the choice of GMM models for the current ShakeMap configuration (Michelini et al., 2020), we adopt the technique of leave-one-out cross-validation analysis (Tomczak, 1998; Hofierka et al., 2007; Worden et al., 2010). The test quantifies the ShakeMap algorithm's accuracy in predicting the station's ground motion model. The strategy is applied separately for each IM under consideration (i.e., PGA, PGV, SA at 0.3s, 1.0s and 3.0s).

To apply the leave-one-out analysis, we need to define a reference data set of earthquakes to be tested. Next, for each earthquake and each recording station, we apply the following procedure iteratively: i) we remove the station under consideration from the dataset; ii) with the remaining stations, we compute the ShakeMap at the location of the station under consideration; iii) we calculate the difference in logarithmic scale between the value predicted by ShakeMap at the station and the actual value recorded for each of the 5 IMs.

For the definition of the validation data set, we focused on earthquakes that fall within the shallow active crustal region (SACR), as defined by Michelini et al. (2020), for the Italian tectonic zonation. The reasons that led us to select only those events that fall within this zone are attributable to the fact that the new model of spatial correlation is calibrated using ITA10 as a reference GMM and that in SACR, the Italian implementation of ShakeMap uses ITA10. Fig. 11 summarizes the main characteristics of the implemented validation data set. A total of 106 earthquakes were analyzed, with 6378 stations (see the table **ESUPP3** in the supplementary material for detail) . The number of recording stations range from a maximum of 201 for the October 30, 2016, earthquake to a minimum of 2 stations for a magnitude 3.9 earthquake near Frosinone in 2008. The magnitude ranges from a minimum of 3.5 to a maximum of 6.5, and the depth is included in the range 3-34 km for earthquakes from 1997 to 2018. In the analysis, we considered only stations with a distance (epicentral or Joyner–Boore distance, depending on the extended fault's availability for the earthquake under consideration) from the epicentre that was no more than 200km. For the generation of the maps, the IMs for earthquakes with $M \geq 4$ have been downloaded from the ESM database while, for events with $M < 4$, from the INGV web services. Similarly, we obtained the finite-fault information through the web-services of the ESM and ITACA databases. We used (partly) different datasets than the one adopted in the analysis, and this choice introduced some independence between the results.

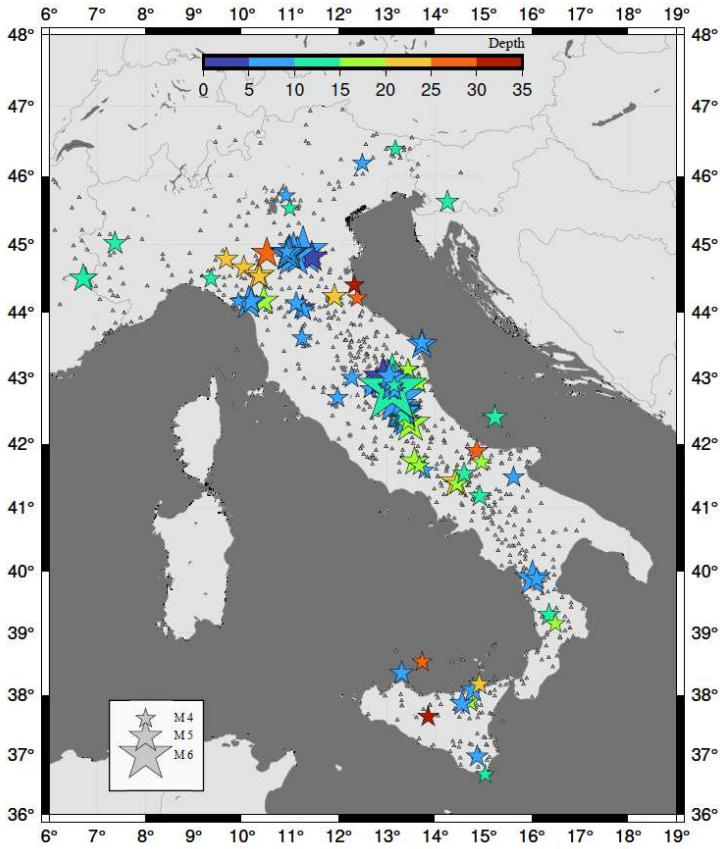

Figure 12. Map of Italian events and stations used for the validation data set. The earthquakes (star markers) are scaled with magnitude and coloured according to the hypocentral depth. The grey triangles are the stations used for the analysis.

Ultimately, for each of the models shown in Table 1, we have opportunely modified the ShakeMap code that deals with calculating spatial correlation, defining the parameters *r1* and *r2* appropriately, and launching the leave-one-out analysis on the 106 earthquakes. Fig. 12 shows the results. The results are presented as differences between observed and predicted IMs through boxplot representations. The same results are resumed in Table 2.

Figure 13 shows that the median value for all the IMs is close to zero for both tested models, indicating no significant systematic bias. Going more specifically, we have that the model of LB13, which is the one currently implemented in ShakeMap, is the one with a median closer to zero. In addition, Table 2 shows a mean and a slightly lower standard deviation for all IMs analyzed for LB13. Regarding the median values, SA 3.0s, contrary to the other IMs, shows results closer to 0 for the analyses proposed in this study than LB13.

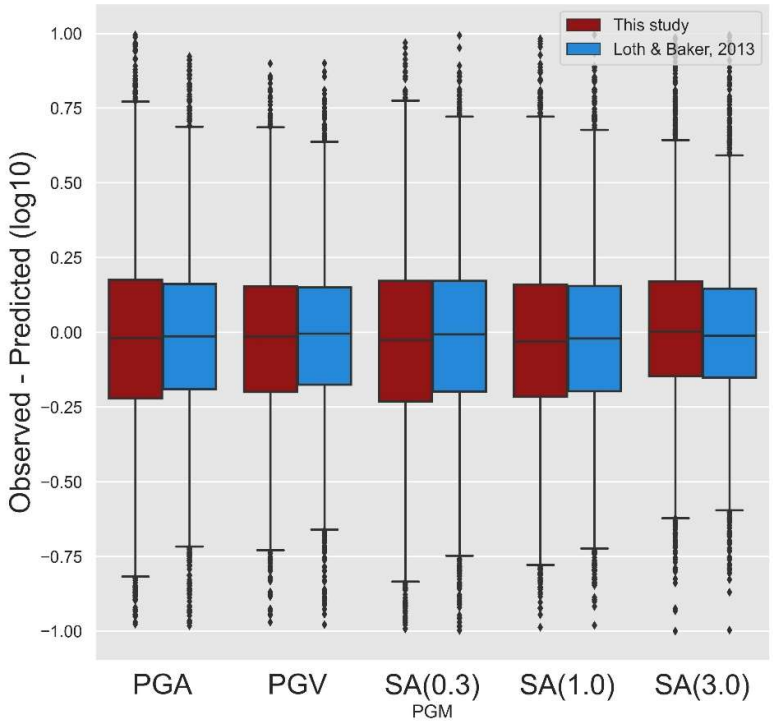

Figure 13. Boxplot diagram of the differences between the base-10 logarithm of observed and ShakeMap predicted values for the entire dataset used in the analysis (106 earthquakes) per the SACR in Italy for the five different modes and the five IMs (Peak Ground Motion, PGM). The units for peak ground acceleration (PGA) and spectral acceleration (SA) are log (percent-g) and for peak ground velocity (PGV) are logcm/s. The boxplot indicates the median values and spans over the first quartile (25 percentile) and third quartile (75 percentile).

Table 2. Median, 25 percentile and 75 percentile as shown in Fig. 12 for the leave-one-out analysis for the two models analysed. For completeness, the table reports the mean and the standard deviation values.

	Loth & Baker (2013)				
	25 perc	**50 perc (median)**	**75 perc**	**mean**	**std**
PGA	-0.190	**-0.013**	0.162	-0.015	0.273

PGV	-0.175	**-0.004**	0.151	-0.012	0.249
SA(0.3)	-0.198	**-0.006**	0.172	-0.014	0.285
SA(1.0)	-0.197	**-0.020**	0.155	-0.018	0.271
SA(3.0)	-0.151	**-0.012**	0.146	0.002	0.236
	This study				
	25 perc	**50 perc (median)**	**75 perc**	**mean**	**std**
PGA	-0,221	**-0,020**	0,176	-0,024	0,306
PGV	-0,199	**-0,013**	0,155	-0,021	0,266
SA(0.3)	-0,230	**-0,026**	0,172	-0,031	0,309
SA(1.0)	-0,215	**-0,031**	0,160	-0,024	0,287
SA(3.0)	-0,146	**0,003**	0,171	0.020	0,261

7. Conclusions

Our outcomes show that the obtained *range* values for Italy are significantly different from those predicted by the LB13 both at short and long periods (-35% and -64%, respectively, with reference to the non-stationary model). Still, these differences do not reflect in a clear improvement of the Shakemap prediction performance assessed via cross-validation despite the improved fitting performance on the semi-variograms of well-recorded events. This result is not obvious as we expect a model calibrated at the regional scale on a well-sampled dataset to produce significantly more constrained estimates than global-scale models, such as LB13. The possible reasons can be related to the following aspects:

- at short-periods ($T \leq 1s$), the estimates of the correlation length are affected by large variability, as shown by the comparison with other Italian correlation models (EI and HG). This may reflect the variability of the calibration datasets from the median predictions of the reference GMM. As a consequence, the estimates of the *range* are

558 highly variable from one spatial model to another and are not able to capture the regional differences in ground
559 motion properties.
560 - at the longest period (T=3s), the five models produce less variable results and the *range* estimates of the Italian
561 models show slightly better performance than the global LB13 model, in terms of median predictions. This trend
562 may suggest that the correlation distance in the long-period is more representative of regional ground motion
563 characteristics, as also evidenced by more consistent patterns relative to the Italian models considered, although
564 the improvement remains negligible.

565 Such low sensitivity of the predictive performance provided by ShakeMap to the correlation distance may also depend
566 on the fact that the Italian data are affected by heterogeneous geologic and geophysical characteristics reflected in highly
567 variable properties of ground shaking throughout Italy. In such a case, a national-scale model may not be sufficient to
568 explain the spatial variability with reference to individual scenarios. On these bases, the calibration of a new spatial
569 correlation model for Italy, as the one proposed here and related to an existing GMM, is unable to resolve regional features
570 compared to the global correlation distances of LB13. More accurate predictions may be achieved through a spatial
571 correlation model specifically calibrated on the residuals of an *ad-hoc* GMM updated to the extended dataset used here.
572 Also, the regional differences observed in the spatial correlation parameters could be better explained by adopting regional
573 or nonergodic GMMs (where the systematic components of variability are decomposed). The latter should lead to more
574 accurate predictions by more effective removal of the repeatable source-, path- and site- related effects from the residuals.

575 Further investigations are ongoing to clarify also the role of the simplified assumptions of stationarity and isotropy on our
576 results, as well as to ascertain the presence of eventual bias in the cross-correlations among different spectral ordinates
577 underlying the LB13 model when applied to the Italian dataset. This would imply that the spatial and spectral parts of the
578 cross-correlation function cannot be separated and thus new co-regionalisation matrices should be calibrated for region-
579 specific applications.

580

581 **References**

582 Al-Atik, L., N. Abrahamson, J. J. Bommer, F. Scherbaum, F. Cotton, and N. Kuehn (2010). The variability of ground-
583 motion prediction models and its components, Seismol. Res. Lett. 81, no. 5, 794–801.

584 Baker JW, Chen Y (2020) Ground motion spatial correlation fitting methods and estimation uncertainty. Earthq Eng
585 Struct Dyn. https:// doi. org/ 10. 1002/ eqe. 3322.

586 Banerjee S, Gelfand A, Carlin B. Multivariate spatial modeling. Hierarchical Modeling and Analysis for Spatial Data.
587 C&H/CRC Monographs on Statistics & Applied Probability, Chapman and Hall/CRC, 2004. 0.

588 Bates D. Mächler M. Bolker B., and Walker S. 2015. Fitting linear mixed-effects models using lme4, *J. Stat. Software*
589 **67,** no. 1, 1–48.

590 Bindi, D., Pacor, F., Luzi, L., Puglia, R., Massa, M., Ameri, G., Paolucci, R., 2011. Ground motion prediction equations
591 derived from the Italian strong motion database. Bull. Earthq. Eng. 9 (6), 1899–1920. https://doi.org/10.1007/s10518-
592 011-9313-z.

593 Bindi, D., D. Spallarossa, F. Pacor, Between-event and between-station variability observed in the Fourier and response
594 spectra domains: comparison with seismological models, *Geophysical Journal International*, Volume 210, Issue 2,
595 August 2017, Pages 1092–1104, https://doi.org/10.1093/gji/ggx217

596 Brunelli G., Lanzano G., D'Amico M.C., Felicetta C., Luzi L., Mascandola C., Pacor F., Russo E., Sgobba S. (2022a).
597 ITACAext flatfile [Data set]. Istituto Nazionale di Geofisica e Vulcanologia (INGV). DOI:
598 10.13127/itaca32/itacaext_flatfile.1.0

599 Brunelli G., Lanzano G., Luzi L., Sgobba S. (2022b). Data-driven zonations for modelling the regional source and
600 propagation effects into ground motion models in Italy. Submitted to Soil Dyn. and Earth. Eng.

601 CEN, 2004. EN 1998–1:2004 Eurocode 8: Design of Structures for Earthquake Resistance—Part 1: General Rules,
602 Seismic Actions and Rules for Buildings. European Committee for Standardization, Brussels.

603 Chen, Y., Baker, J., 2019. Spatial correlations in cybershake physics-based ground motion simulations. Bull. Seismol.
604 Soc. Am. 1–17. https://doi.org/10.1785/0120190065.

605 Chen, F.W. and C. W. Liu. Estimation of the spatial rainfall distribution using inverse distance weighting (IDW) in the
606 middle of Taiwan,Paddy Water Environ, 2012, 10, 209-222.

607 Colavitti, L., Lanzano, G., Sgobba, S., Pacor, F., & Gallovič, F. (2022). Empirical evidence of frequency-dependent
608 directivity effects from small-to-moderate normal fault earthquakes in Central Italy. Journal of Geophysical Research:
609 Solid Earth, 127, e2021JB023498. https://doi.org/10.1029/2021JB023498

610 Crowley, H., Stafford, P., Bommer, J.J., 2008. Can earthquake loss models be validated using field observations? J.
611 Earthq. Eng. 12 (7), 1078–1104.

612 Dreger, D. S., 2003, TDMT_INV: Time Domain Seismic Moment Tensor INVersion, International Handbook of
613 Earthquake and Engineering Seismology, Volume 81B, p 1627.

614 Esposito S.,Iervolino I.. (2011) PGA and PGV spatial correlation models based on European multi-event datasets, Bulletin
615 of the Seismological Society of America, 101(5): 2532–2541.

616 Esposito, S., Iervolino, I., 2012. Spatial correlation of spectral acceleration in European data. Bull. Seismol. Soc. Am.
617 102 (6), 2781–2788. https://doi.org/10.1785/0120120068.

618 Goda, K., Hong, H.P., 2008. Spatial correlation of peak ground motions and response spectra. Bull. Seismol. Soc. Am.
619 98 (1), 354–365.

620 Heresi, P., and Miranda, E. (2019). "Uncertainty in intraevent spatial correlation of elastic pseudo-acceleration spectral
621 ordinates." Bulletin of Earthquake Engineering, 17(3), 1099-1115.https://doi.org/10.1785/0120070078.

622 Huang C, Galasso C. 2019. Ground-Motion Intensity Measure Correlations Observed in Italian Strong-Motion Records.
623 Earthquake Engineering & Structural Dynamics; 48(15): 1634–1660. doi: 10.1002/eqe.3216

624 Hofierka, J., T. Cebecauer, and M. Šúri (2007). Optimisation of inter- polation parameters using cross-validation, in
625 Digital Terrain Modelling, R. J. Peckam and G. Jordan (Editors), Springer Berlin Heidelberg, Berlin, Heidelberg, 67–82.

626 Infantino M, Smerzini C, Lin J (2021) Spatial correlation of broadband ground motions from physics-based numerical
627 simulations. Earthq Eng Struct Dyn. https:// doi. org/ 10. 1002/ eqe. 3461

628 Jayaram, N., Baker, J.W., 2009. Correlation model for spatially distributed ground-motion intensities. Earthquake Eng.
629 Struct. Dynam. 38. https://doi.org/10.1002/eqe.

630 Lanzano, G., Luzi, L., Pacor, F., Felicetta, C., Puglia, R., Sgobba, S., D'Amico, M., 2019. A revised Ground-Motion
631 Prediction Model for Shallow Crustal Earthquakes in Italy. Bull. Seismol. Soc. Am. 109 (2), 525–540.

632 Lanzano G., Sgobba S., Luzi L., Puglia R., Pacor F., Felicetta C., D'Amico M., Cotton F., Bindi D. (2018). The pan-
633 European Engineering Strong Motion (ESM) flatfile: compilation criteria and data statistics. Bulletin of Earthquake
634 Engineering, 17(2), 561-582, DOI: 10.1007/s10518-018-0480-z

635 Loth, C., and Baker, J. W. (2013). “A spatial cross-correlation model of ground motion spectral accelerations at multiple
636 periods.” Earthquake Engineering & Structural Dynamics, 42, 397-417.

637 Loth, C. and Baker, J.W. (2020), Erratum: A spatial cross-correlation model for ground motion spectral accelerations at
638 multiple periods. Earthquake Engng Struct Dyn, 49: 315-316. https://doi.org/10.1002/eqe.3233

639 Matheron, G., 1962. Traité de géostatistique appliquée. 1 (1962). Editions Technip.

640 Menafoglio A. Sgobba S. Lanzano G., and Pacor F. 2020. Simulation of seismic ground motion fields via object-oriented
641 spatial statistics with an application in Northern Italy, Stoch. Environ. Res. Risk Assess. 32, no. 12, 3421–3437.

642 Michelini A. Faenza L. Lauciani V., and Malagnini L. 2008. ShakeMaps implementation in Italy, Seismol. Res. Lett. 79,
643 688–697.

644 Michelini, A., Faenza, L., Lanzano, G., Lauciani, V., Jozinović, D., Puglia, R., Luzi, L., 2020. The New ShakeMap in
645 Italy: Progress and advances in the last 10 Yr. Seismol. Res. Lett. https://doi.org/10.1785/0220190130.

646 Oliver, M.A., Webster, R., 2014. A tutorial guide to geostatistics: Computing and modelling variograms and kriging. In:
647 Catena. 113. Elsevier B.V., pp. 56–69. https://doi. org/10.1016/j.catena.2013.09.006.

648 Pagani, M., D. Monelli, G. Weatherill, L. Danciu, H. Crowley, V. Silva, P. Henshaw, L. Butler, M. Nastasi, L. Panzeri,
649 M. Simionato, D. Vigano; OpenQuake Engine: An Open Hazard (and Risk) Software for the Global Earthquake Model.
650 Seismological Research Letters 2014; 85 (3): 692–702. doi: https://doi.org/10.1785/0220130087

651 Paolucci R. Pacor F. Puglia R. Ameri G. Cauzzi C., and Massa M. 2011. Record processing in ITACA, the new Italian
652 strong-motion database, in Earthquake Data in Engineering Seismology, Akkar S. Gulkan P., and Van Eck T. (Editors),
653 Geotechnical, Geological and Earthquake Engineering Series, Vol. 14, Springer, Dordrecht, The Netherlands, 99–113.

654 Park, J., Bazzurro, P., Baker, J.W., 2007. Modeling spatial correlation of ground motion Intensity measures for regional
655 seismic hazard and portfolio loss estimation. Appl. Stat. Prob. Civil Eng. 1–8.

656 Pondrelli, S. (2002). European-Mediterranean Regional Centroid-Moment Tensors Catalog (RCMT) [Data set]. Istituto
657 Nazionale di Geofisica e Vulcanologia (INGV). https://doi.org/10.13127/rcmt/euromed

Schiappapietra E, Douglas J (2020). Modelling the spatial correlation of earthquake ground motion: Insights from the literature, data from the 2016–2017 Central Italy earthquake sequence and ground-motion simulations. Earth-science reviews, vol 203. https:// doi. org/ 10. 1016/j. earsc irev. 2020. 103139

Schiappapietra, E., Douglas, J. (2021). Assessment of the uncertainty in spatial-correlation models for earthquake ground motion due to station layout and derivation method. Bull Earthquake Eng 19, 5415–5438 (2021). https://doi.org/10.1007/s10518-021-01179-w

Schiappapietra E, Smerzini C (2021). Spatial correlation of broadband earthquake ground motion in Norcia (Central Italy) from physics-based simulations. Bull Earthq Eng. https://doi.org/10.1007/s10518-021-01160-7

Schiappapietra, E., Stripajová, S., Pažák, P., Douglas, J., Trendafilosk, G. (2022). Exploring the impact of spatial correlations of earthquake ground motions in the catastrophe modelling process: a case study for Italy. Bull Earthquake Eng 20, 5747–5773. https://doi.org/10.1007/s10518-022-01413-z

Sedaghati F, Pezeshk S (2017). Partially nonergodic empirical ground-motion models for predicting horizontal and vertical PGV, PGA, and 5% damped linear acceleration response spectra using data from the Iranian Plateau. Bull Seismol Soc Am 107:934–948.

Sgobba, S., Lanzano, G., Pacor, F., Puglia, R., D'Amico, M., Felicetta, C., Luzi, L., (2019). Spatial Correlation Model of Systematic Site and Path Effects for Ground-Motion Fields in Northern Italy. Bull. Seismol. Soc. Am. https://doi.org/10.1785/0120180209.

Sgobba S, Lanzano G, Pacor F (2021) Empirical non-ergodic shaking scenarios based on spatial correlation models: an application to Central Italy. Earthq Eng Struct Dyn. https:// doi. org/ 10. 1002/ eqe. 3362

Sokolov, V., Wenzel, F., Kuo-Liang, W., 2010. Uncertainty and spatial correlation of earthquake ground motion in Taiwan. TAO. Terr. Atmos. Ocean. Sci. 21 (6), 9. https://doi.org/10.3319/TAO.2010.05.03.01(T).

Sokolov, V., Wenzel, F., 2011. Influence of spatial correlation of strong ground motion on uncertainty in earthquake loss estimation. Earthq. Eng. Struct. Dyn. 40, 993–1009. https://doi.org/10.1002/eqe.1074.

Stafford P. J. 2014. Crossed and nested mixed-effects approaches for enhanced model development and removal of the ergodic assumption in empirical ground-motion models, Bull. Seismol. Soc. Am. 104, no. 2, 702–719.

683 Tomczak, M., (1998). Spatial interpolation and its uncertainty using automated anisotropic inverse distance weighting
684 (IDW)-cross- validation/jackknife approach, J. Geogr. Inf. Decision Anal. 2, no. 2, 18–30.

685 Verros, S.A., Wald, D.J., Worden, C.B., Hearne, M., Ganesh, M., 2017. Computing spatial correlation of ground motion
686 intensities for ShakeMap. Comput. Geosci. 99, 145–154. https://doi.org/10.1016/j.cageo.2016.11.004.

687 Weatherill, G.A., et al., 2015. Exploring the impact of spatial correlations and uncertainties for portfolio analysis in
688 probabilistic seismic loss estimation. Bull. Earthq. Eng. 13 (4), 957–981. https://doi.org/10.1007/s10518-015-9730-5.

689 Worden, C.B., E.M. Thompson, J.W. Baker, B.A. Bradley, N. Luco, and D.J. Wald (2018). Spatial and Spectral
690 Interpolation of Ground Motion Intensity Measure Observations, Bull. Seism. Soc. Am. 108(2), 866-875. doi:
691 https://doi.org/10.1785/0120170201

692 Worden, C.B., E. M. Thompson, M. Hearne, and D.J. Wald (2020). ShakeMap Manual Online: technical manual, user's
693 guide, and software guide, U. S. Geological Survey. http://usgs.github.io/shakemap/. DOI:
694 https://doi.org/10.5066/F7D21VPQ.

695 Worden, C. B., D. J. Wald, T. I. Allen, K. Lin, D. Garcia, and G. Cua (2010). A revised ground-motion and intensity
696 interpolation scheme for ShakeMap, Bull. Seismol. Soc. Am. 100, 3083–3096.

697 Zerva, A., Zervas, V., 2002. Spatial variation of seismic ground motions: an overview. Appl. Mech. Rev. 55 (3), 271.
698 https://doi.org/10.1115/1.1458013.

699 Zimmaro, P., G. Scasserra, J. P. Stewart, T. Kishida, G. Tropeano, M.Castiglia, and P. Pelekis (2018). Strong ground
700 motion characteristicsfrom 2016 Central Italy earthquake sequence, Earthq. Spectra 34,no. 4, 1611–1637, doi:
701 10.1193/091817EQS184M.

STATEMENTS & DECLARATIONS

Fundings

This study was partially funded in the framework of INGV and Dipartimento della Protezione Civile (INGV-DPC) AGREEMENT B2 2019–2021, within the Task related to ShakeMap implementation in Italy.

Competing Interests

The authors have no relevant financial or non-financial interests to disclose.

Author Contributions

All authors contributed to the material preparation, data collection and analysis. Study conception and design was performed by Sara Sgobba. The first draft of the manuscript was written by Sara Sgobba and all authors commented on previous versions of the manuscript. All authors read and approved the final manuscript.

Data Availability: The original dataset (Brunelli et al., 2022a) used to calibrate the spatial correlation model proposed in this study is accessible at the following URL: https://itaca.mi.ingv.it/ItacaNet_32/#/products/itacaext_flatfile. Velocimetric records are automatically downloaded from the European Integrated Data Archive (EIDA http://www.orfeus-eu.org/eida/eida.html) within the ESM database. Input data for the ShakeMap validation test are available at ESM (https://esm-db.eu/#/home), ITACA (https://itaca.mi.ingv.it/ItacaNet_32/#/home) and INGV (http://terremoti.ingv.it/webservices_and_software).